Monthly Notices of the ROYAL ASTRONOMICAL SOCIETY

MNRAS **529,** 1802–1813 (2024) https://doi.org/10.1093/mnras/stae616
Advance Access publication 2024 February 28

The *TESS*-SPOC FFI target sample explored with *Gaia*

Lauren Doyle,[1,2]★ David J. Armstrong,[1,2] Daniel Bayliss,[1,2] Toby Rodel[1,2,3] and Vedad Kunovac[1,2]

[1]*Centre for Exoplanets and Habitability, University of Warwick, Coventry CV4 7AL, UK*
[2]*Department of Physics, University of Warwick, Coventry CV4 7AL, UK*
[3]*Astrophysics Research Centre, School of Mathematics and Physics, Queen's University Belfast, Belfast BT7 1NN, UK*

Accepted 2024 February 20. Received 2024 February 16; in original form 2023 October 11

ABSTRACT

The *Transiting Exoplanet Survey Satellite* (*TESS*) mission has provided the community with high-precision times-series photometry for ∼2.8 million stars across the entire sky via the full frame image (FFI) light curves produced by the *TESS* Science Processing Operations Center (SPOC). This set of light curves is an extremely valuable resource for the discovery of transiting exoplanets and other stellar science. However, due to the sample selection, this set of light curves does not constitute a magnitude-limited sample. In order to understand the effects of this sample selection, we use *Gaia* Data Release 2 (DR2) and Data Release 3 (DR3) to study the properties of the stars in the *TESS*-SPOC FFI light-curve set, with the aim of providing vital context for further research using the sample. We report on the properties of the *TESS*-SPOC FFI targets in Sectors 1–55 (covering Cycles 1–4). We cross-match the *TESS*-SPOC FFI targets with the *Gaia* DR2 and DR3 catalogues of all targets brighter than *Gaia* magnitude 14 to understand the effects of sample selection on the overall stellar properties. This includes *Gaia* magnitude, parallax, radius, temperature, non-single star flags, luminosity, radial velocity, and stellar surface gravity. In total, there are ∼16.7 million *Gaia* targets brighter than $G = 14$, which when cross-matched with the *TESS*-SPOC FFI targets leaves ∼2.75 million. We investigate the binarity of each *TESS*-SPOC FFI target and calculate the radius detection limit from two detected *TESS* transits that could be detected around each target. Finally, we create a comprehensive main-sequence *TESS*-SPOC FFI target sample that can be utilized in future studies.

Key words: catalogues – surveys – planets and satellites: general – stars: fundamental parameters.

1 INTRODUCTION

Since its launch in 2018 April, the *Transiting Exoplanet Survey Satellite* (*TESS*; Ricker et al. 2015) has transformed the field of stellar and exoplanetary physics. *TESS* has successfully discovered scores of transiting exoplanets, including planets transiting very bright host stars (e.g. Gandolfi et al. 2018; Huang et al. 2018), small radius planets (e.g. Gilbert et al. 2020; Oddo et al. 2023), multiplanet systems (e.g. Leleu et al. 2021), and planets around young stars (e.g. Newton et al. 2019; Battley, Pollacco & Armstrong 2020; Mann et al. 2022). At the time of writing, *TESS* is currently in its second extended mission, observing Sectors 70–83. This marks the sixth year of *TESS* observations observing some of the ecliptic and the Northern hemisphere for a third time.[1] The extended *TESS* mission allows for the detection of longer period transiting planets (e.g. Gill et al. 2020; Lendl et al. 2020) and also opens the door into the search for stellar activity cycles (e.g. Davenport, Mendoza & Hawley 2020; Doyle et al. 2022).

TESS is composed of four cameras, each of which maps onto an array of four CCDs. The combined field of view (FOV) is 24° × 94°, which makes up one sector where each is observed for ∼27 d. For a full description of the *TESS* mission, see Ricker et al. (2015). There are various data collection modes for *TESS*; however, for this work we exclusively focus on the full frame images (FFIs). For Sectors 1–26, the FFIs were acquired every 30 min, whereas for Sectors 27–56 the cadence of the FFIs was improved to every 10 min. From Sector 57 onwards, the cadence was improved even further to 200 s, making this mode comparable to the 2-min postage stamp targeted sample. The *TESS* Science Processing Operations Center (SPOC; Jenkins et al. 2016) is responsible for the *TESS* science pipeline that is based on the very successful *Kepler* pipeline. From the second year of the *TESS* mission, the SPOC began processing FFI light curves for up to 160 000 targets per sector (Caldwell et al. 2020). All pixel and light-curve data for the *TESS*-SPOC FFI target sample are contributed as High Level Science Products (HLSPs) on the *Mikulski Archive for Space Telescopes* (*MAST*),[2] where they are publicly available. Due to the fact that the *TESS*-SPOC FFIs constitute a large and homogeneously processed set of light curves, they have been an extremely valuable resource for the community, used for a wide range of studies, including planet discoveries (e.g. Gilbert et al. 2020; Eisner et al. 2021; Yee et al. 2022), statistical studies (e.g. Bryant, Bayliss & Van Eylen 2023), and binary star studies (e.g. IJspeert et al. 2021; Prša et al. 2022).

★ E-mail: lauren.doyle@warwick.ac.uk
[1]https://tess.mit.edu/tess-year-6-observations/
[2]https://archive.stsci.edu/

In this paper, we explore the physical parameters of the stars in the *TESS*-SPOC FFI target sample using observations from the *Gaia* mission (Gaia Collaboration 2016), from both *Gaia* Data Release 2 (DR2; Gaia Collaboration 2018) and Data Release 3 (DR3; Gaia Collaboration 2023). In Section 2, we detail the full *Gaia* and SPOC samples and discuss how we cross-match them to achieve our final *TESS*-SPOC FFI target sample. Here, we also look at the spread of observed *TESS* sectors for each target. In Section 3, we determine the radius detection limit from two detected *TESS* transits that could be detected around each *TESS*-SPOC FFI target and also look at the distribution of *TESS* Objects of Interest (TOIs) in the colour–magnitude diagram of the *TESS*-SPOC FFI target sample. In Section 4, we investigate the binarity of the sample using the non-single star (NSS) and renormalized unit weight error (RUWE) flags in the *Gaia* data. Finally, in Section 5 we isolate main-sequence stars in the *TESS*-SPOC FFI target sample as a prime sample for further future statistical studies that wish to focus on dwarf stars.

2 TARGET SAMPLES

The precise method of sample selection for stars to be included in the *TESS*-SPOC FFI light curves results in a set of targets that is close to, but not quite, a magnitude-limited sample. In this section, we detail both the *TESS*-SPOC FFI target sample and a *Gaia* magnitude-limited sample, and investigate the difference between the two.

2.1 *TESS*-SPOC FFI sample

The *TESS*-SPOC FFI targets are selected on a set of criteria designed to maximize scientific goals and minimize the impact on processing times in the SPOC context (Caldwell et al. 2020). The target selection is made in the following way.

(i) All 2-min targets are selected (∼20 000 per sector).
(ii) Targets are selected with an H magnitude ≤10 or with a distance ≤100 pc, provided the crowding metric ≥0.5 and the *TESS* magnitude ≤16.
(iii) Targets with *TESS* magnitude ≤13.5, log surface gravity (log g) ≤3.5, and crowding metric ≤0.8.

The crowding metric, as defined in the SPOC and *Kepler* pipelines (Smith et al. 2016), is the fraction of flux in the optimal aperture that is due to the target star. For example, a crowding metric of 0.8 means 80 per cent of the flux within the aperture is from the target star; therefore, in (ii) and (iii) above, the crowding metric must be greater than 0.5 and 0.8, respectively, for the target to be selected.

Targets are selected on a per CCD basis, following the priority order set out above. A limit of 10 000 targets per CCD is placed on the allocation to ensure that the processing time does not impact the operations of the SPOC. Given *TESS* contains a total of 16 CCDs, this results in a limit of 160 000 stars for the *TESS*-SPOC FFI light curves for a given sector. For many sectors, this limit is indeed reached, which in practice means that there will be stars in the third select category above which are not included. In such cases, the targets are selected by apparent magnitude, with the brightest stars being prioritized. The split of *TESS*-SPOC FFI targets for each sector in Cycle 1 is shown in Fig. 1. From this, it is clear the 2-min targets account for 10–15 per cent, the M dwarf sample with $d \leq 100$ pc accounts for 3–4 per cent, and the vast majority are targets with *TESS* magnitude ≤13.5, log surface gravity ≤3.5, and crowding metric ≤0.8. It is also worth noting that there is a dip in the overall number of *TESS*-SPOC FFI targets between Sectors 8 and 12, which is a result of the galactic plane being within the *TESS* FOV, resulting in fewer targets meeting the crowding metric cut of 0.8.

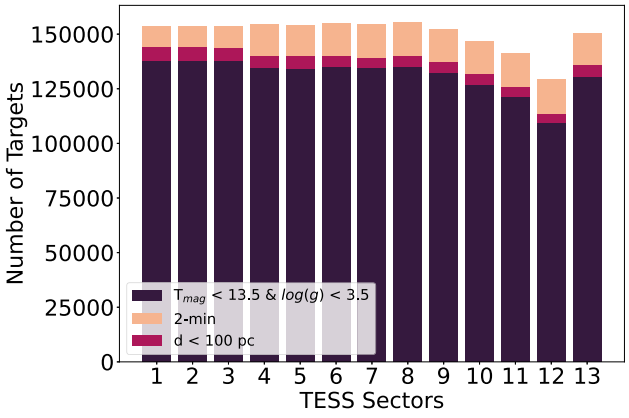

Figure 1. A bar chart showing the split of *TESS*-SPOC FFI targets in each sector for Cycle 1. The top of the bar (in orange) are the targets that are also observed in 2-min cadence (10–15 per cent), in the middle (pink) are the targets with $d \leq 100$ pc (3–4 per cent), and at the bottom (in purple) the remaining targets that represent those with $T_{\rm mag} \leq 13.5$, $\log g \leq 3.5$, and crowding metric ≤0.8.

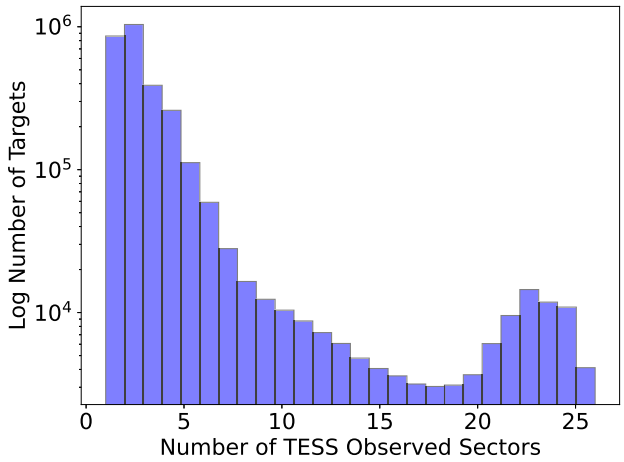

Figure 2. The histogram of the observed *TESS* sectors of each *TESS*-SPOC FFI target in a logarithmic scale. This shows the spread of observed sectors in the sample with the majority being observed between Sectors 2 and 3. There is a further peak in the histogram at Sector 23, which represents stars within the *TESS* continuous viewing zone.

In this study, we select all *TESS*-SPOC FFI targets that were observed in Sectors 1–55, covering Cycles 1–4. This is due to *TESS* currently observing in Cycle 5/6 where all data are not yet available at the time of writing. Furthermore, from Cycle 5 onwards *TESS* will observe FFIs in a 200-s cadence. By using observations from Cycles 1–4, we have observations covering both the Northern and Southern hemispheres twice, creating a complete sample that will allow for repeatability of findings between sectors and cycles.

For all of the *TESS*-SPOC FFI targets in Sectors 1–55, we gather their *TESS* Input Catalog (TIC) ID, right ascension, declination, and their *Gaia* DR2 identifier that comprises a total of 2891 782 individual targets. We also determine the number of *TESS* sectors each individual target has been observed for and show the results in Fig. 2. It can be seen that the majority of targets are observed between Sectors 2 and 3, where there is a peak in the histogram.

There is a further peak at around Sector 23, which represents targets within the ecliptic poles that lie within the *TESS* continuous viewing zone. Lastly, we also extract the precision of each target from the header of the SPOC light curve and use this information in Section 3.

2.2 *Gaia* sample

The *Gaia* mission (Gaia Collaboration 2016) is part of the science programme of the European Space Agency (ESA) and was launched in 2013 December. The scientific goals of *Gaia* are extensive where the key aim is to measure the distances, positions, space motions, and physical properties of one billion stars in our Galaxy. *Gaia* provides a map of our Galaxy for the first time, complete for all stars brighter than $G = 20$. This provides detailed information on all stars in the *TESS*-SPOC FFI target sample set out in Section 2.1. For this study, we use data released by *Gaia* DR2 (Gaia Collaboration 2018) and DR3 (Gaia Collaboration 2023), accessing the data through a table access protocol (TAP) query using ADQL in TOPCAT (Taylor 2005).

Gaia DR2 is based on data collected during the first 22 months of the *Gaia* mission. This release made the leap to high-precision parallax and proper motion measurements for over one billion stars, and is a major advancement on DR1 with regards to the completeness and accuracy. Homogeneous multiband photometry and large-scale radial velocity observations at the bright ($G \leq 13$) end were also made available in the DR2 release. *Gaia* DR3 is based on Early Data Release 3 (EDR3, an earlier release in 2021; Gaia Collaboration 2021) where astrometry and broad-band photometry were not updated from DR2. The full *Gaia* DR3 was released in 2022 with updated radial velocities, spectra from the radial velocity spectrograph, astrophysical parameters for sources based on the blue and red prism photometer (BP and RP) spectra, amongst much more. This release was based on data gathered over the first 34 months of the mission and provides significant improvement in both the precision and accuracy of measurements. At the time of writing *Gaia* DR3 is the most recent *Gaia* data release, and the next *Gaia* data release (DR4) will not be released before the end of 2025.[3]

We use the *Gaia* DR3 parallaxes to estimate the absolute *Gaia* magnitude in the G band for individual stars following the methods of Babusiaux et al. (2018). In addition to retrieving the DR3 sample, we also fetched the DR2 identifiers (`source_id`) that are very useful in cross-matching the *TESS*-SPOC FFI sample. This is because the TIC (v8.2; Stassun et al. 2019) IDs are associated with the *Gaia* DR2 identifiers. Between *Gaia* DR2 and DR3 there are changes to the identifiers just as there are between *Gaia* DR1 and DR2. This is as a result of the source lists becoming progressively more stable and of higher spatial resolution over the course of the *Gaia* mission.

The stellar astrophysical parameters contained within the *Gaia* DR3 are composed of atmospheric properties, evolutionary parameters, metallicity, individual chemical element abundances, and extinction parameters, along with other characterization such as equivalent widths of the Hα line and activity index for cool active stars (see Vallenari et al. 2023, for full details). In *Gaia* DR2, median radial velocities for ∼7 million sources were presented, along with estimates of the stellar effective temperature, extinction, reddening, radius, and luminosity for between 77 and 161 million sources (see Gaia Collaboration 2018, for full details). *Gaia* DR3 contained newly determined radial velocities for about 33.8 million stars with $G_{\rm RVS}$ (median of the single-transit radial velocity spectrometer measurements) ≤ 14 and with $3100 \leq T_{\rm eff} \leq 14\,500$ K. Therefore, we use the radial velocity, parallax, and $\log g$ measurements from DR3 and the effective temperature, stellar radius, and luminosity from DR2.

The *Gaia* DR2 effective temperatures are estimated from two distance-independent colours $G_{\rm BP} - G$ and $G - G_{\rm RP}$. Machine learning is used to come up with a non-parametric model for the colour–temperature relation where the training sample contains targets with $T_{\rm eff} = 3000$–$10\,000$ K. Therefore, there is no *Gaia* target with a temperature listed outside of this range. The luminosities from *Gaia* DR2 are estimated using the FLAME software package (part of the APSIS data processing system; see Bailer-Jones et al. 2013, for further details) utilizing relations between the effective temperature and *Gaia* absolute magnitude. Finally, the stellar radius is then estimated using the effective temperature and luminosity.

2.3 *TESS*-SPOC FFI and *Gaia* cross-matched sample

In order to cross-match the *TESS*-SPOC FFI target sample with *Gaia*, we first create a magnitude-limited sample of *Gaia* stars in DR3 where the relative precision on the parallax is better than 20 per cent (following Babusiaux et al. 2018) and $G < 14$. This brightness cut is used as the *TESS*-SPOC FFI target sample predominantly comprises stars brighter than $T_{\rm mag} = \sim 13.5$ (see Section 2.1 for further details). Furthermore, the number of *Gaia* targets fainter than $G = 14$ increases significantly, making it more difficult and time-consuming to access and download the *Gaia* sample. We cross-matched the *TESS*-SPOC FFI targets to the *Gaia* magnitude-limited sample using the *Gaia* DR2 source identifiers. This produced a total of 2744 013 cross-matches, leaving 147 769 *TESS*-SPOC FFI targets without a match. This deficit results from the two cuts on magnitude (94.7 per cent) and parallax error precision (5.3 per cent) made when creating the *Gaia* magnitude-limited sample. In order to form a more complete sample of the *TESS*-SPOC FFI targets, we cross-matched the remaining 147 769 with the *Gaia* DR3 catalogue directly using their right ascension and declination from the TIC and a radius search of 8 arcsec. This produced a further 146 604 *TESS*-SPOC FFI targets with *Gaia* DR3 parameters where the 1165 missing targets were a result of high proper motion on the order of hundreds of milliarcseconds per year. There were a number of targets that were flagged as duplicates by *TESS* and these have been removed. The original cross-match and the additional targets from the radius search make the full final *TESS*-SPOC FFI target sample with a total count of 2890 583 individual targets.

Fig. 3 shows the spread of absolute and mean *Gaia* magnitudes in the *TESS*-SPOC FFI target sample compared with the underlying *Gaia* sample for $G < 14$. All stars that fall into the *TESS* FOV and are brighter than $T = 6$ (but not so bright as to cause CCD saturation) are selected for 2 min cadence light curves (Stassun et al. 2018). Therefore, since all of these 2 min cadence targets are also chosen as *TESS*-SPOC FFI targets (see selection criteria set out in Section 2.1), the *TESS*-SPOC FFI target sample is complete for almost all stars with $G < 6$.

For stars fainter than $G = 6$, the *TESS*-SPOC FFI target sample is incomplete, and the degree of incompleteness is shown in Fig. 4. In this plot, the black line represents the percentage of completeness within the *TESS*-SPOC FFI target sample compared to the *Gaia* magnitude-limited sample. The red line then shows the completeness of the *TESS*-SPOC FFI main-sequence sample (defined in Section 5) compared to the *Gaia* magnitude-limited main-sequence sample that is created in the same way as the SPOC sample with a cut on surface gravity $\log g > 3.5$. From this, it is clear the full *TESS*-SPOC

[3] https://www.cosmos.esa.int/web/gaia/release

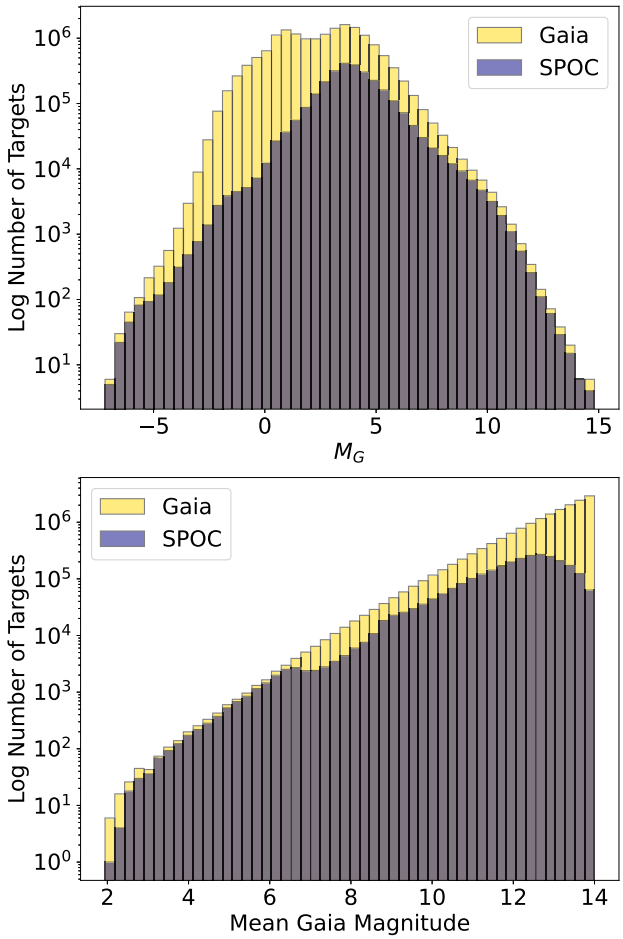

Figure 3. A histogram of the absolute *Gaia* magnitude and mean *Gaia* magnitude from DR3 for both the *Gaia* sample (yellow/background distribution) and the *TESS*-SPOC FFI target sample (navy/forefront distribution).

FFI target sample is almost complete for stars with $G < 6$ where it drops off suddenly. There is also a peak in completeness around $G = 9$ that could correspond to large *TESS* Guest Investigator (GI) programmes as these targets are observed in 2-min cadence and so are automatically included in the *TESS*-SPOC FFI target sample. For the main-sequence sample there is a much higher completeness across the whole magnitude range that drops off towards the end at $G = 13$.

Using the *Gaia* DR3 magnitudes, parallaxes, and colours we are able to plot the full Hertzsprung–Russell diagram (HRD) for the *TESS*-SPOC FFI target sample that can be seen in Fig. 5. This shows the diversity of stellar classes and types that are present within the *TESS*-SPOC FFI target sample. The majority of the samples are on the main sequence. At 0.75 mag above the main sequence, a subtle binary track can be seen that is due to near-equal mass main-sequence binary stars. Also evident on the HRD are the spread of subgiants and giants, a clump of blue hot subdwarfs, and the faint white dwarf sequence. All of these classes of stars are present in the *TESS*-SPOC FFI target sample due to being selected as 2-min cadence targets. This selection is due to the stars being very bright ($T < 6$) or through *TESS* GI programmes that target specific classes of stars such as white dwarfs in G04137 and G022028 by J. J. Hermes, subgiants in G022099 by J. Tayar, and hot subdwarfs in G022141 by B. Barlow.

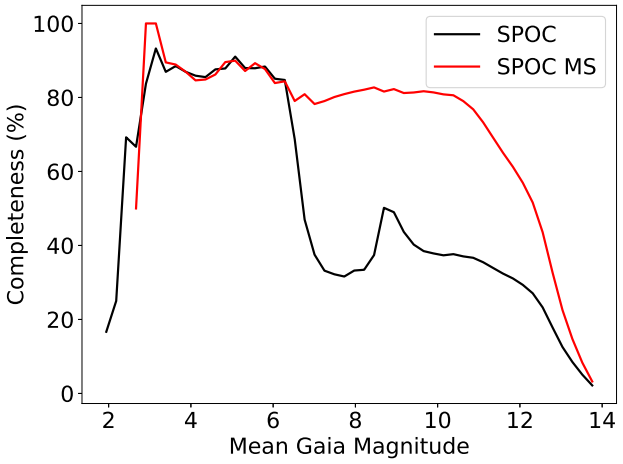

Figure 4. The completeness of the *TESS*-SPOC FFI target sample in comparison to the *Gaia* magnitude-limited sample. The black line represents the full *TESS*-SPOC FFI sample compared to the full *Gaia* sample, and the red line is the *TESS*-SPOC FFI main-sequence sample compared to the *Gaia* main-sequence sample defined in Section 5.

Fig. 6 shows the ratio of *TESS*-SPOC FFI targets to the magnitude-limited *Gaia* sample in the format of an HRD with a grid resolution of 2000 × 2000. Yellow colouring indicates the *TESS*-SPOC FFI target sample has the same number of targets as the underlying *Gaia* sample – i.e. the *TESS*-SPOC FFI sample is approximately complete. Dark blue colouring indicates there are very few *TESS*-SPOC FFI targets compared with the underlying *Gaia* sample – i.e. the *TESS*-SPOC FFI sample is very incomplete. It is evident that the *TESS*-SPOC FFI target sample is most complete for fainter main-sequence low-mass stars and also across the main sequence in general. The *TESS*-SPOC FFI target sample is most incomplete for evolved/giant stars. This is a result of the *TESS* 2-min targets being largely free of giant stars [see discussions in Stassun et al. 2018, on the assembly of the Candidate Target List (CTL)]. The reason for this was that *TESS* is an exoplanet transit survey mission, and transits around subgiants or giants are much shallower compared to equivalent transits around main-sequence stars. Additionally, the criteria in which additional *TESS*-SPOC FFI targets are selected (see Section 2.1) include nearby stars ($d < 100$ pc) and exclude low surface gravity stars ($\log g > 3.5$), both of which will naturally exclude horizontal and giant branch stars.

The distribution of *Gaia* stellar properties for the *TESS*-SPOC FFI target sample is set out in Fig. 7. The distribution in radial velocity is a Gaussian with a peak at 0 km s^{-1}, inline with the expectation for a large set of nearby stars selected from across the entire sky. The distribution of effective temperatures is also sharply peaked at around 6000 K, reflecting the fact that the sample is largely made up of solar-type main-sequence stars. There is a small bump in the distribution at approximately 3500 K, which comes about both from the selection of M dwarfs in the 2-min frames and the selection of additional M dwarfs in the *TESS*-SPOC FFI selection for nearby stars ($d < 100$). Similarly the $\log g$ and stellar radius distributions largely reflect the fact that dwarf stars on the main sequence make up the bulk of the sample. Fig. 8 shows the distributions of distances that peak at around 400 pc, with 90 per cent of targets having a distance of 850 pc or less. Furthermore, we also plot the distribution of distances for ∼200 000 *Kepler* targets observed in Q1 where there is a peak at 1000 pc. It is important to note here that *TESS* is observing many more stars at 1000 pc compared to *Kepler*, however, from 1500 pc

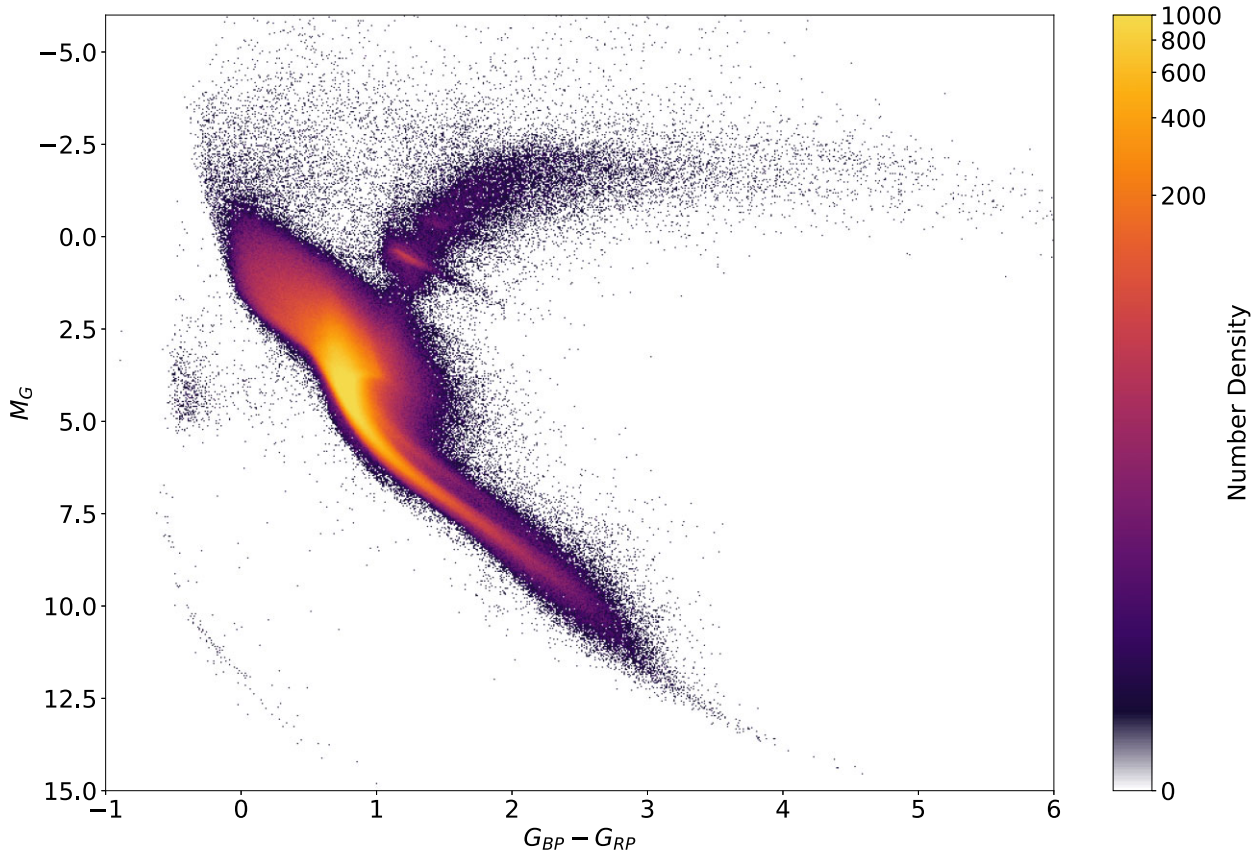

Figure 5. The colour–magnitude diagram of all *TESS*-SPOC FFI targets from *TESS* Sectors 1–55. All colours along with the parallax, used to determine the absolute *Gaia* magnitude, were taken from the *Gaia* DR3 catalogue. The colour scale represents the log of the density of stars.

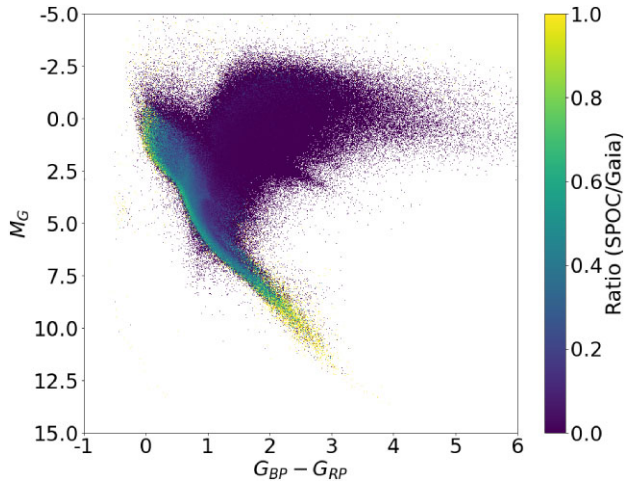

Figure 6. Colour–magnitude diagram where the colour scale shows the ratio between *TESS*-SPOC FFI and *Gaia* targets. Yellow (Ratio = 1.0) represents both samples having the same number of targets and dark blue (Ratio = 0.0) where targets are in the *Gaia* sample but not the *TESS*-SPOC FFI sample.

onwards *Kepler* begins to take over observing more stars at a further distance. A small peak can be seen for $d < 100$ pc, which is due to the selection of nearby stars in 2-min sample and in the *TESS*-SPOC FFI selection criteria.

3 EXOPLANET DETECTIONS WITH *TESS* DATA

The primary science goal of *TESS* is to discover planets smaller than Neptune that transit stars bright enough to enable follow-up spectroscopic observations. It is this combination of photometry and spectroscopy that can provide properties of planetary systems such as planet radii, planet masses, and atmospheric compositions. Therefore, the SPOC data products were developed with exoplanet transit searches as a focus.

3.1 *TESS* targets of interest

Potential transiting planets are found by searching for periodic flux decreases, known as Threshold-Crossing Events (TCEs), in both the SPOC 2-min light curves created from postage stamps and 30-min cadence FFI light curves from the Quick-Look Pipeline, which is another *TESS* data processing pipeline. These TCEs are then examined by the *TESS* Science Office (TSO) to identify planet candidates that would benefit from follow-up observations. Light curves are run through software to eliminate any obvious non-planetary signals where the remaining are manually vetted and listed as a TOI for follow-up observations. Any TCEs that fall under other categories from eclipsing binaries to variable stars are not included in the TOI Catalog (Guerrero et al. 2021), but are included in the comprehensive TCE Catalog available on MAST. At the time of writing there are currently 6687 TOIs that have been followed up and confirmed or are still awaiting further observations to confirm the planetary system.

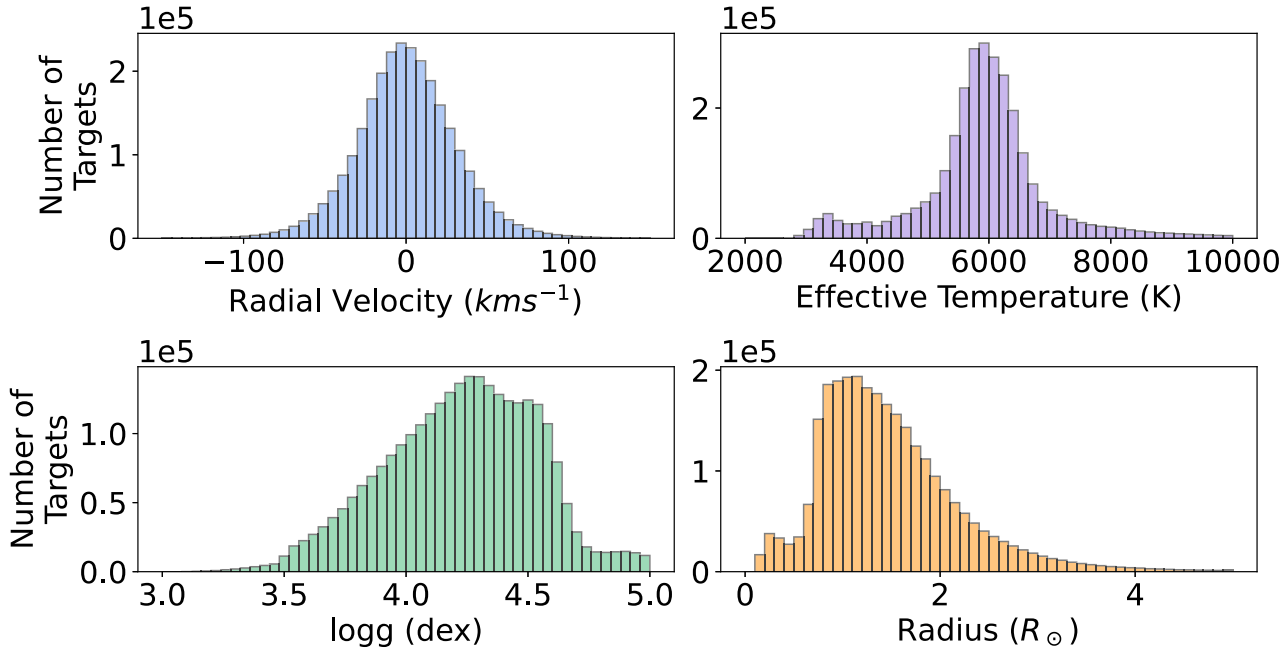

Figure 7. Stellar properties of the *TESS*-SPOC FFI target sample. The radial velocity measurements are from *Gaia* DR3, and the remaining properties are taken from the *Gaia* DR2 catalogue. The range shown in each plot was cut to enable the distribution to be seen. The percentage of the sample that lies out of the axes is as follows: radial velocity 3.7 per cent, temperature 1.8 per cent, log g 2.5 per cent, and radius 1.9 per cent.

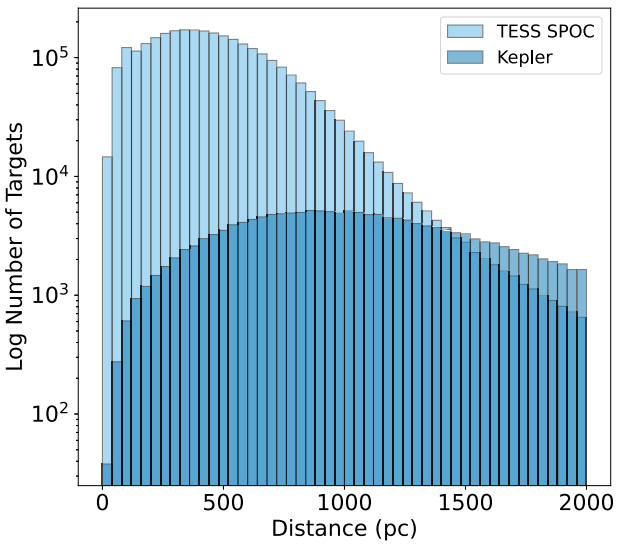

Figure 8. The log distribution of distances for the *TESS*-SPOC FFI target sample, taken from the parallaxes of *Gaia* DR3 (light blue/background distribution), showing those with distances less than 2000 pc. We also overplot the *Kepler* distances of ∼200 000 targets from Q1 (dark blue/forefront distribution). The range shown has been cut to enable the distribution to be seen, therefore, 0.6 per cent of *TESS* and 22 per cent of *Kepler* targets lie outside the axes.

In fig. 6 of Guerrero et al. (2021), candidates from the *TESS* primary mission are overplotted on a *Gaia* sample. In a similar manner, we took the list of all currently known TOIs and cross-matched it with the *TESS*-SPOC/*Gaia* FFI target list. This produced a total of 3950 known TOIs that have SPOC FFI data. For the remaining 2737 targets we cross-matched them directly with the *Gaia* DR3 catalogue to obtain the *Gaia* parameters for each. This was done using the right ascension and declination of each target and a cone search of 6°. This then allowed us to plot the two TOI samples as those with SPOC FFI data (red) and those without (green) in Fig. 9 over top of the SPOC HRD. While it is the 2-min *TESS* light curves that are used by TSO to identify TCEs, each 2-min light curve has a corresponding *TESS*-SPOC FFI light curve (see Section 2.1). In Fig. 9, it can be seen that the majority of TOIs lie within the main sequence with outliers close to the hot subdwarfs and white dwarfs as well as a sample in the horizontal and giant branches. It also provides an indication for *TESS* Cycles 1–4 of which TOIs have been identified using SPOC data. The majority of those with SPOC data lie in the main sequence with the exception of a handful of outliers. This aligns with the strategy of selecting SPOC targets.

3.2 *TESS*-SPOC FFI sensitivity to transit detections

Since detecting transiting exoplanets is the main science goal of the *TESS* mission and each SPOC 2-min light curve is scanned for TCEs, it is worth exploring the sensitivity of the sample light curves to transit detections. Therefore, we explored what would be the radius detection limit from two detected *TESS* transits one could expect to detect for each of the *TESS*-SPOC FFI targets. Hereafter, we refer to this as the two-transit radius detection limit. Note that this is an estimate designed to study the sample, rather than a strict limit for individual targets. Furthermore, we do not consider the number of transits that might be observed in total by *TESS*, therefore, we provide only upper limits on the two-transit detectable planet radius. In other words, smaller planets may be detected with many more transits.

To do this we extracted the precision of each *TESS*-SPOC FFI target taken from the SPOC light-curve header where provided. The photometric precision metric within the SPOC light curves is based on the *Kepler* pipeline (Jenkins et al. 2010) and is called the combined differential photometric precision (CDPP). It is defined as the root-mean-square of the photometric noise on transit time-scales and is

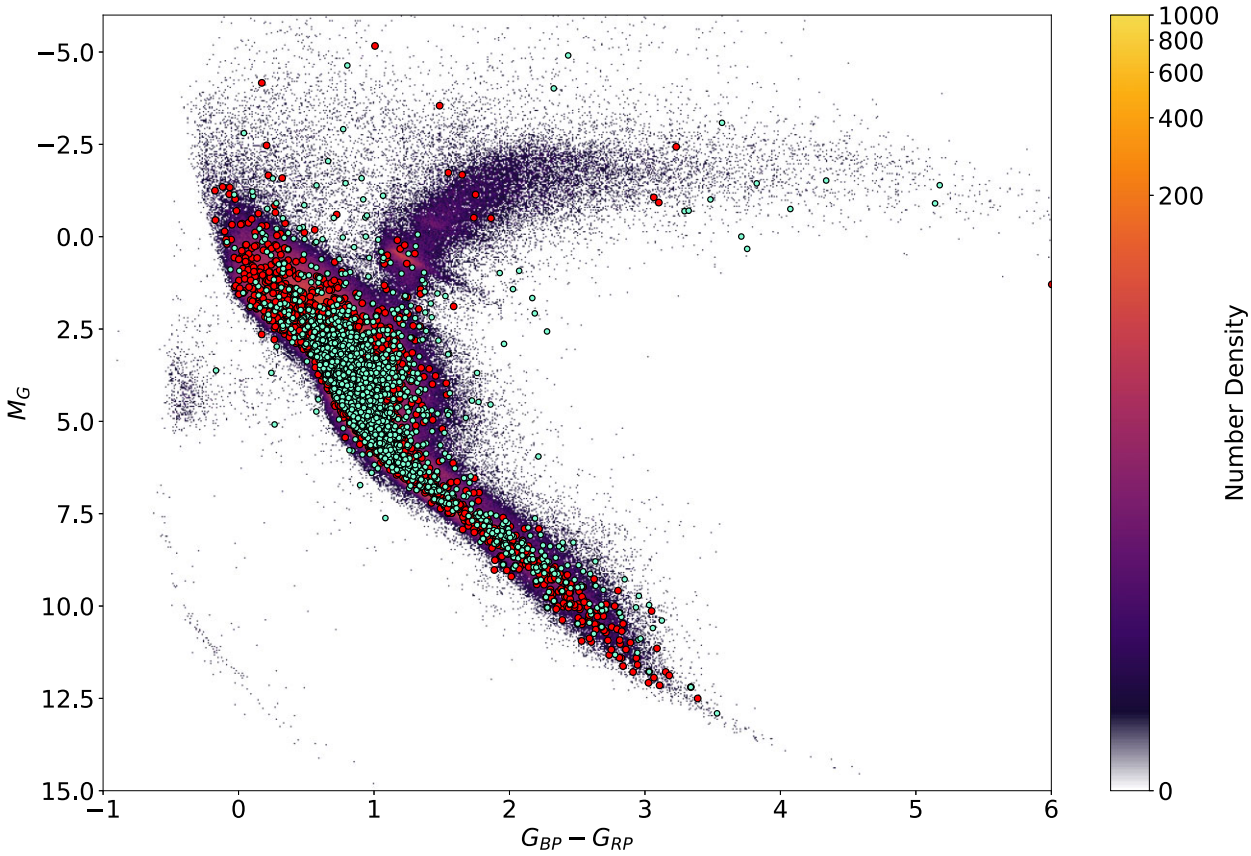

Figure 9. *TESS* TOIs overplotted as circles onto the colour–magnitude diagram of all *TESS*-SPOC FFI targets. Those with SPOC data are plotted in red (4270) with the remaining TOIs with no SPOC data overplotted in green (2417).

used by the SPOC when searching for periodic transit searches. For our purposes, we use the CDPP of each target, the Multiple Event Statistic (MES) threshold of 7.1 from SPOC as a measure of signal-to-noise ratio used to claim a detection and assume a transit duration of 2.7 h that has been taken as the median transit duration of all the known TOIs. While MES is not identical to signal-to-noise ratio, it is similar according to Jenkins (2002) and Twicken et al. (2018). We use this to be consistent with the SPOC pipeline, however, other studies such as Sullivan et al. (2015) and Kunimoto et al. (2022) have used the threshold in signal-to-noise ratio of 7.3. This is put together to estimate the two-transit radius detection limit ($R_{\rm pmin}$) from two *TESS* transits in equation (1):

$$R_{\rm pmin} = 10^{-6} \times R_* \sqrt{\frac{\rm SNR\sigma}{\sqrt{T_{\rm dur}/2}}}, \quad (1)$$

where SNR is the signal-to-noise ratio threshold of $7.1/\sqrt{2}$ to account for a two-transit detection, $T_{\rm dur}$ is the average TOI transit duration of 2.7 h (divided by 2 since we are using the 2-h CDPP values), R_* is the stellar radius, and σ is the CDPP precision of the light curve.

In Fig. 10, we plot individual HRDs colour coded by the two-transit radius detection limit to show the spread in the context of the stellar properties for each *TESS*-SPOC FFI target. Fig. 11 shows the same data of the two-transit radius detection limit as a distribution, where the peak of the histogram lies at $\sim 6 R_\oplus$. Both plots are split up according to planetary radius corresponding to our Solar system planets as: Earths/super-Earths in the range $0.5 < R_\oplus \leq 2.0$, mini-Neptunes in the range $2.0 < R_\oplus \leq 4.0$, gas giants in the range $4.0 < R_\oplus \leq 27.0$, and non-planetary companions in the range $27.0 < R_\oplus \leq 100.0$. As can be expected the Earth/super-Earth population is mostly found amongst the lower main-sequence population and mini-Neptunes are found around stars on the whole of the main sequence. For the larger gas giants these tend to be spread slightly on the main sequence but are also found around stars that are evolved on the horizontal and giant branches. In Section 6, we compare our findings with that of other planet detection estimate results, namely that if Kunimoto et al. (2022).

4 NON-SINGLE STARS/BINARIES

Binary stars can be observed from Earth as visual/resolved, spectroscopic, eclipsing, and astrometric. These gravitationally bound star systems are considered to be important as they allow the masses of stars to be determined (see Söderhjelm 1999; Al-Wardat et al. 2021). It is expected that up to 50 per cent of all stars are in binary systems with some even as triple or higher multiple systems. However, this fraction is higher for hotter stars, can decrease with higher metallicity, and also is related to age and distance (Tian et al. 2018). As a result of this, *Gaia* provides its own parameters to indicate the potential binary nature of a given star.

First, to indicate if any of our stars are members of binary systems we used the RUWE from the *Gaia* DR3 Catalog (see Lindegren et al. 2018, for full details). The RUWE is a goodness-of-fit measurement of the single-star model to the target astrometry that is highly sensitive to the photocentre motion of binaries (see Belokurov et al. 2020).

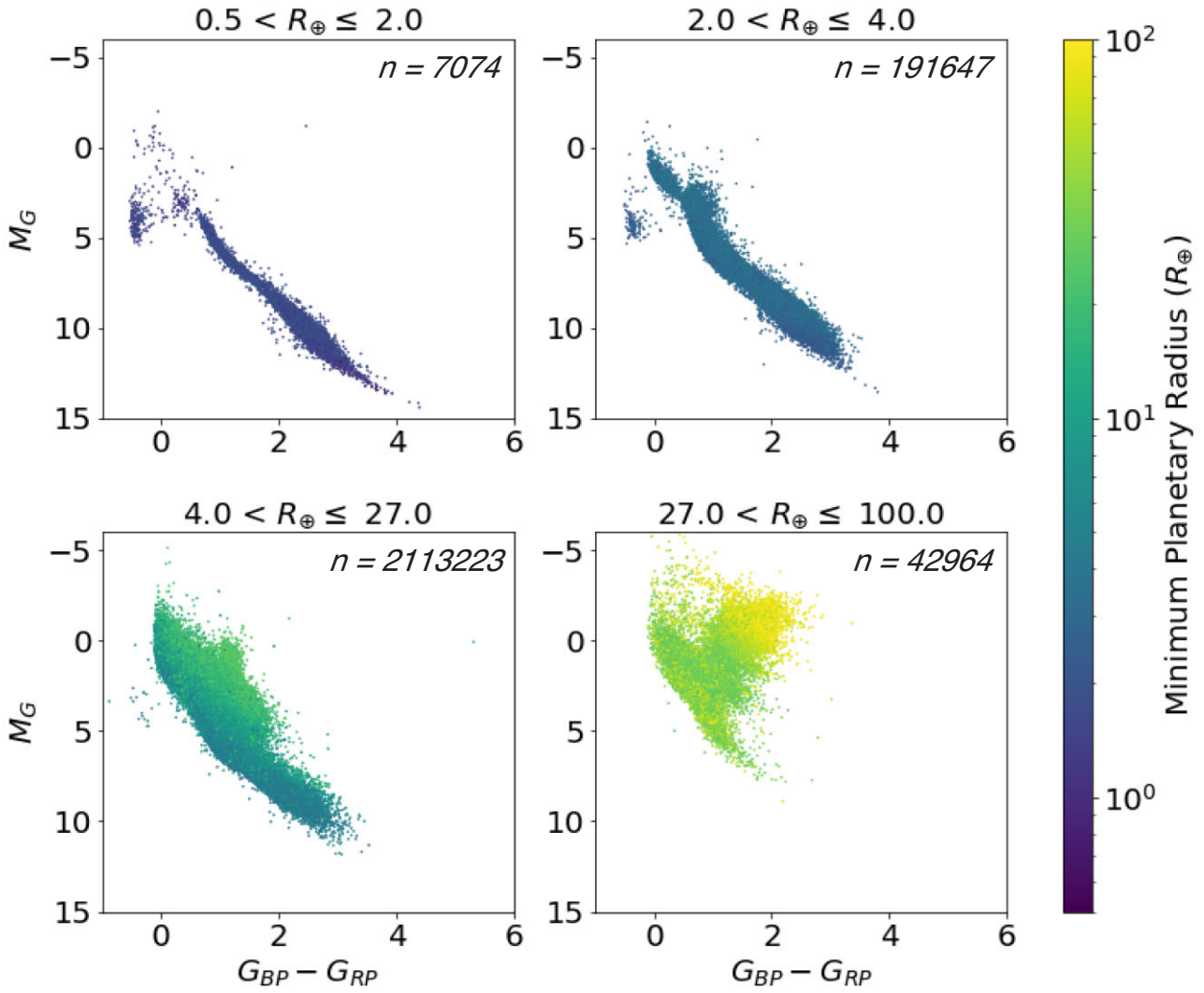

Figure 10. Colour–magnitude diagrams showing the distribution of the calculated two-transit radius detection limit of an exoplanet that could be detected around each *TESS*-SPOC FFI target. Each plot has been split up according to planetary radius with Earths/super-Earths in the range $0.5 < R_\oplus \leq 2.0$, mini-Neptunes in the range $2.0 < R_\oplus \leq 4.0$, gas giants in the range $4.0 < R_\oplus \leq 27.0$, and non-planetary companions in the range $27.0 < R_\oplus \leq 100.0$. The number of each category in each subplot is given in the top right-hand corner. The radius calculation was determined using the average TOI duration of 2.7 h as the transit duration, assuming a circular orbit and using the signal-to-noise ratio of $\mathbf{7.1/\sqrt{2}}$.

Overall, the RUWE is expected to be around 1.0 for all sources where the single-star model provides a good fit to the astrometric measurements where a RUWE $\geq$ 1.4 could indicate the star is non-single. In total, there are 540 038 *TESS*-SPOC FFI targets with a RUWE $\geq$ 1.4 that could be considered as potential binary systems, which are all plotted in Fig. 12. In Fig. 12, the RUWE value of each *TESS*-SPOC FFI target is shown as the colour of each point on the HRD. Here the more yellow the data point, the higher the RUWE value of the target and the more likely it is in a binary system. Overall, there is a spread of targets with RUWE $\geq$ 1.4 across the whole of the HRD including the main sequence, red giant and horizontal branches, and even hot subdwarfs and white dwarfs. However, the majority of stars with very high RUWE values are those along the main sequence. This follows what we know about binary systems where approximately half of F, G, and K stars are expected to be in a binary system (Raghavan et al. 2010; Moe & Di Stefano 2017).

In addition to the RUWE value, *Gaia* also provides a non-single star (NSS) flag as an indication of the binary nature of a target. This flag indicates the target has been identified as an NSS by the *Gaia* Data Processing and Analysis Consortium (DPAC). As such, the observations have been put through tests of various binary orbit models. The NSS solutions are then kept when significant and fit with an acceptable quality. For those where binarity was detected in several instruments, a combination fit is considered to improve the precision of the orbital parameters. Therefore, the NSS flag is organized in three main flags that inform on the nature of the NSS model. They are as follows: Flag 1 is an astrometric binary; Flag 2 is a spectroscopic binary; and Flag 4 is an eclipsing binary. Some of the NSS flags represent models that are combinations of these three, for example, Flag 5 would represent the combination of Flag 1 and Flag 4 that informs us that there is an astrometric and eclipsing binary solution (full details of all the flags are in Table 1).

In total, 196 391 *TESS*-SPOC FFI targets have an NSS flag with the combinations within these shown in Table 1. The majority of targets have NSS Flag 1 that indicates an astrometric binary. In Fig. 12, each of the individual NSS flags is overplotted onto the HRD

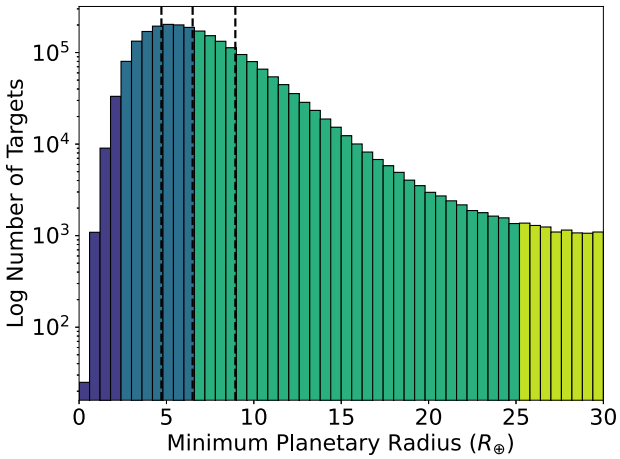

Figure 11. A log histogram distribution of the calculated two-transit radius detection limit of an exoplanet that could be detected around each *TESS*-SPOC FFI target. The radius calculation was determined using the median transit duration of all TOIs as the transit duration, assuming a circular orbit and using the signal-to-noise ratio of $7.1/\sqrt{2}$. The bars are colour coded according to the planetary radius with Earths/super-Earths in the range $0.5 < R_\oplus \leq 2.0$ as dark blue, mini-Neptunes in the range $2.0 < R_\oplus \leq 4.0$ as blue/green, gas giants in the range $4.0 < R_\oplus \leq 27.0$ as green, and non-planetary companions in the range $27.0 < R_\oplus \leq 100.0$ as yellow.

to show the spread. It can be seen that the majority lie on the main sequence and red giant/horizontal branches with only two close to the white dwarf region. Furthermore, the higher NSS flags seem to correlate around the top of the main sequence in the region of the O, B, and A stars. This seems reasonable as more than 70 per cent of OBA stars exist in binary systems (Sana et al. 2012). This could be a result of the average number of companions per OB primary being at least three times higher than that of low-mass stars with 0.5 companions on average (Zinnecker 2003; Grellmann et al. 2013).

Overall, both the *Gaia* binarity parameters have flagged 18.68 per cent from RUWE and 6.79 per cent from NSS in the *TESS*-SPOC FFI targets. In total, 157 206 *TESS*-SPOC FFI targets have both a RUWE $\geq$ 1.4 and NSS flag that equates to 5.43 per cent of the sample. Therefore, a total of 579 223 *TESS*-SPOC FFI targets have either a RUWE $\geq$ 1.4 or an NSS that equates to 20.04 per cent of the sample. This is a considerable fraction of the target sample; therefore, for future detailed analysis of these potential binary targets, the *Gaia* information could be used to infer more details on the binary nature. This could be useful when considering searching for planets around these stars and/or looking at variability.

5 ISOLATING THE SPOC MAIN SEQUENCE

One of the main goals of this paper was to create a comprehensive main-sequence *TESS*-SPOC FFI target sample that can be utilized in other studies. In the creation of the *TESS*-SPOC FFI target sample (Caldwell et al. 2020), targets were added up to 160 000 for each sector using the criteria of surface gravity $\log g > 3.5$. This added dwarfs and subgiants to the sample that matches our criteria for selecting the main sequence. Therefore, we apply this criterion to the whole of the *TESS*-SPOC FFI target sample that leaves us with 2319 308 main-sequence targets. The full HRD of this sample can be seen in Fig. 13 where the main sequence is clearly identified and the horizontal and giant branches are no longer seen. The properties for each target, including the *Gaia* DR3 properties, are listed in Table 2, which is also available as a machine-readable table online.

6 DISCUSSION AND CONCLUSIONS

In this paper, we have explored the properties of the *TESS*-SPOC FFI target sample by utilizing the *Gaia* DR3 catalogue. From this, we have identified a well-defined main-sequence *TESS*-SPOC FFI target sample that is available to the community for future studies (see Table 2). The aim behind this is to standardize a sample that can be used for large surveys that are based on the *TESS*-SPOC FFI data that are publicly available.

First, we created our final *TESS*-SPOC FFI target sample by cross-matching the *TESS*-SPOC FFI target sample with *Gaia* DR3 using the *Gaia* DR2 source identifier. Any *TESS*-SPOC FFI targets that were missed out were matched using a cone search with *Gaia* on the

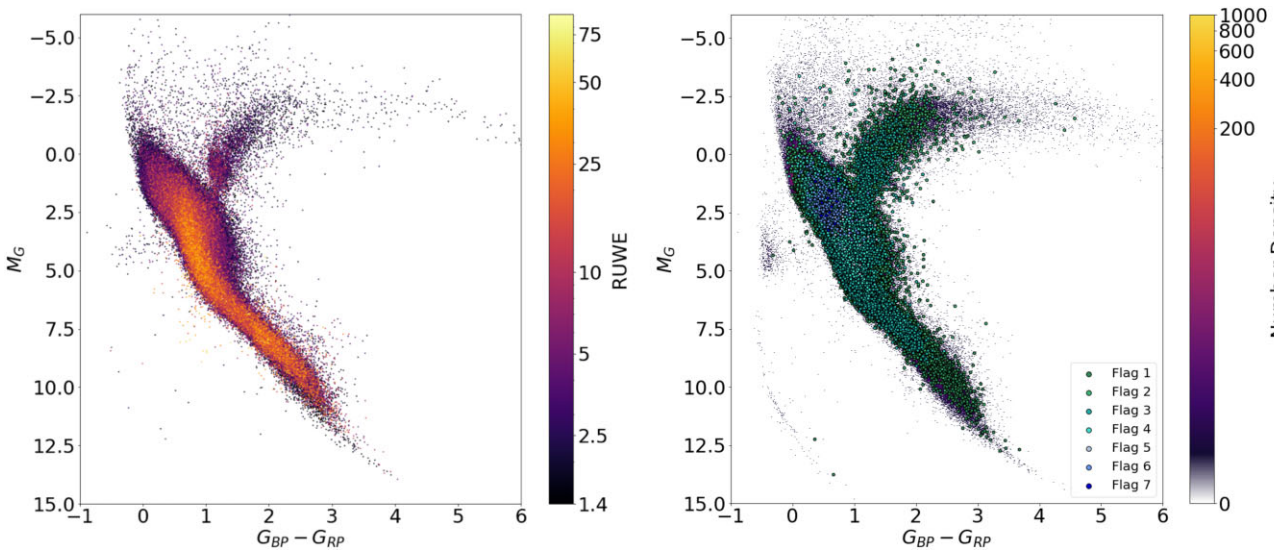

Figure 12. The colour–magnitude diagram of all *TESS*-SPOC FFI targets from *TESS* Sectors 1–55. The left plot is colour coded according to *Gaia* RUWE, and the right plot has the *Gaia* NSS flags overplotted. In each plot the higher RUWE and NSS flags are plotted on the top in order to be seen given the large sample size. Full details of what each NSS flag represents are given in Table 1.

Table 1. The number of each *TESS*-SPOC FFI targets that fall into each of the NSS flags along with the descriptor for each. The final column shows the percentage of the *TESS*-SPOC FFI target sample of 2890 583 sources.

NSS flag	Descriptor	Number of *TESS*-SPOC targets	Percentage of *TESS*-SPOC FFI target sample
1	Astrometric binary (AB)	107 271	3.71
2	Spectroscopic binary (SB)	56 626	1.96
3	AB and SB	30 642	1.06
4	Eclipsing binary (EB)	1488	0.05
5	AB and EB	54	0.002
6	EB and SB	296	0.01
7	AB, SB, and EB	14	0.0005

right ascension and declination to form a more complete sample (see Section 2.3 for the full details). The comparisons between both the *Gaia* sample and the *TESS*-SPOC FFI target sample with regards to absolute magnitude show a stronger spread among main-sequence targets for SPOC (see Fig. 3). The mean absolute *Gaia* magnitude for the *Gaia* sample is 2.6 and for the *TESS*-SPOC FFI target sample is 3.9 (see Fig. 3), which falls inline with the selection criteria for SPOC and is unsurprising.

For each of our *TESS*-SPOC FFI targets, we used the CDPP from the SPOC FFI light curves to estimate the two-transit radius detection limit of an orbiting exoplanet. In order to do this, we also had to make a few assumptions: (i) the transit duration was set to 2.7 h (median transit duration of all known TOIs) and (ii) the signal-to-noise ratio threshold was set to $7.1/\sqrt{2}$. In Kunimoto et al. (2022), they use simulations of *TESS* data along with injection and recovery tests to determine the number of detectable planets around 8.5 million AFGKM stars from the *TESS* CTL, v8.01. Their stellar sample was taken from the CTL keeping only targets that were classified as dwarfs and removing all giants. This is different from the *TESS*-SPOC FFI target sample that, as seen from Fig. 5, has targets from main-sequence dwarfs to red giants and white dwarfs. In total, over 7 yr of *TESS* observations, Kunimoto et al. (2022) predict a planet yield of 12 519 ± 678, with 8426 ± 525 planets detectable from the primary mission and first extended mission (i.e. Years 1–4). It is important to note that they have an upper limit of 16 $R_\oplus$ for AFGK stars and 4 $R_\oplus$ for M stars within their injection and recovery tests. Overall, they find that G-type stars are the most common hosts and half of the *TESS* planet detections consist of gas giants with radii greater than 8 $R_\oplus$.

From our *TESS*-SPOC FFI main-sequence target sample, 41 per cent of targets are G-type stars, which is in agreement with our median $T_{\rm eff}$ of 5933 K; therefore, the majority of our two-transit radius detection limits are from host stars that are G-type. Furthermore, we also find that 38 per cent of our two-transit radius detection limits are giants with $R_{\rm p} > 8$ $R_\oplus$. We also have a peak in our distribution of detectable planetary radii that falls at ∼6 $R_\oplus$. While it is important to note we are not producing a yield estimate, it is reassuring that similarities are found among our two-transit radius detection limits. We do not perform any injection and recovery tests as it is beyond the scope of this paper. Furthermore, Kunimoto et al. (2022) used a model planet distribution that is a function of planet

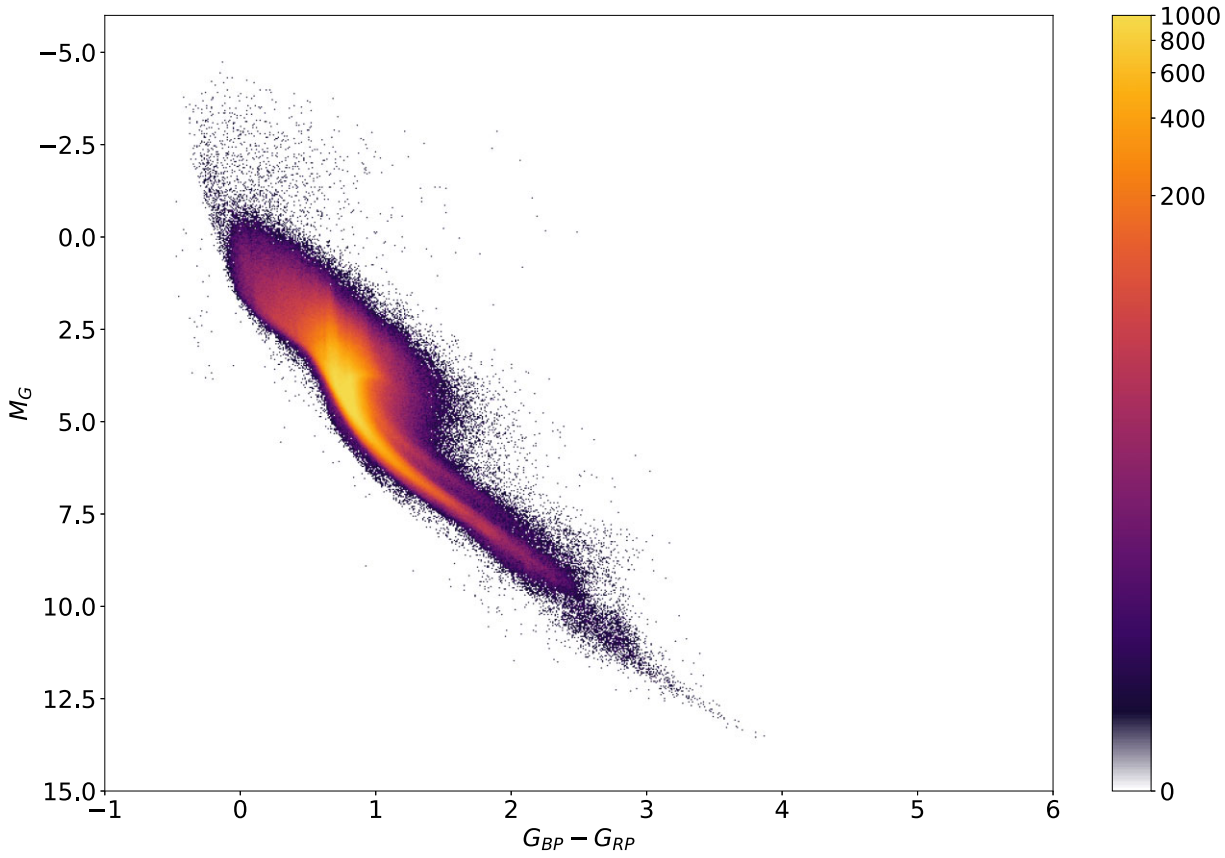

Figure 13. The *Gaia* colour–magnitude diagram of the main-sequence *TESS*-SPOC FFI target sample. These targets were isolated by filtering on $\log g > 3.5$ that resulted in a final main-sequence *TESS*-SPOC FFI target sample of ∼2.3 million.

Table 2. A small subsample of the main-sequence *TESS*-SPOC FFI target sample. In total, we show a selection of 13 columns out of the 21 available for each target. Amongst these we include the TIC and *Gaia* DR3 IDs and also the estimated detectable two-transit radius detection limit for each target as the last column. This table is available in its entirety in a machine-readable format at CDS, a small subsample is shown here for guidance regarding its form and content.

TIC ID	*Gaia* DR3 source id	RA (°)	Dec. (°)	Parallax (mas)	g mag	M_G	$G_{BP} - G_{RP}$	T_{eff} (K)	log g (cgs)	RUWE	NSS	Two-transit radius ($R_\oplus$)
990573	3803801020782388736	165.46	−0.66	1.64	13.40	4.48	0.91	5569	4.23	1.09	0	9.86
25176115	1991484152278341632	350.97	51.21	6.00	2.65	6.54	1.38	4512	4.48	3.21	1	5.43
66457200	477598718345633920	73.69	61.76	2.66	9.22	1.35	0.29	8121	3.88	0.94	0	7.84
284468412	4559345936350050432	253.24	17.29	5.57	10.85	4.59	0.93	5496	4.29	1.39	2	4.43
420831735	5929340070299722368	251.61	−55.57	1.33	10.81	1.44	0.63	7037	3.46	0.81	0	27.6
⋮	⋮	⋮	⋮	⋮	⋮	⋮	⋮	⋮	⋮	⋮	⋮	⋮

size, orbital period, and host star spectral type to predict their yield. In this study, we only present the detectability, but do not consider how it varies with increasing numbers of transits, where this would lead to smaller planet radii detections. Furthermore, when calculating our two-transit radii we assume uncorrelated Gaussian noise. However, the *TESS*-SPOC pipeline goes to considerable effort to decorrelate the data before any transit detections; therefore, the noise within the light curves is generally not uncorrelated Gaussian noise and does not strictly obey square-root statistics. There is no simple solution to correct for this, but we would just like to make a note here for the reader.

With our cross-matched sample, we explored the *Gaia* properties for the *TESS*-SPOC FFI target sample (see Fig. 7). The median effective temperature of the sample is 5933 K; this lies in the range of G-type stars and is in agreement with our stellar spectral type distribution. Further to this, the median stellar radius is 1.36 $R_\odot$, which is a typical radius for an FGK star. There also appears to be a second bump in radius at ∼0.5 $R_\odot$, which is indicative of low-mass M dwarfs. This can also be seen in distance at ∼100 pc and in effective temperature at ∼3000 K, which all correspond to low-mass M dwarf properties. This is not surprising since *TESS* has a redder bandpass than *Kepler*, making it easier to detect exoplanets around low-mass stars. Furthermore, the increase in M dwarfs with *TESS* can also be attributed to their emphasis in the selection process for SPOC 2-min and SPOC FFI targets (see Section 2.1). With regards to distance, the median was 438 pc with 90 per cent of stars having a distance of 850 pc or less. Finally, the median log g is 4.25, which centres around what we know for the Sun with log g = 4.43 (Gray 2021). There is also a second peak in the log g distribution at 4.5, suggesting a group of high surface gravity stars; however, there is also a small peak at ∼0.3 $R_\odot$. Therefore, it is likely that the peaks in log g of 4.5, T_{eff} of ∼3000 K, and radius of ∼0.3 $R_\odot$ correspond to M dwarfs, which forms part of the SPOC selection process.

Overall, this paper presents the first overview of the *TESS*-SPOC FFI target sample, utilizing data from *Gaia* DR3. We have produced the first HRD of the *TESS*-SPOC FFI target sample showing a wide distribution of targets from the main sequence, red giant branch, white dwarfs, and hot subdwarfs. Furthermore, we have produced a main-sequence *TESS*-SPOC FFI target sample that is publicly available for the community to use in further studies. Given the success of the SPOC pipeline and the planet yield expected from *TESS* going forward, we hope this will encourage a standardized target list to be used when appropriate. Furthermore, we have also estimated the two-transit radius detection limit for each target using *TESS*-SPOC FFI data to inform future planet searches. This may help when developing search strategies for new transiting exoplanets in the future.

ACKNOWLEDGEMENTS

We include data in this paper collected by the *TESS* mission, where funding for the *TESS* mission was provided by the NASA Explorer Program. This work presents results from the European Space Agency (ESA) space mission *Gaia*. *Gaia* data are being processed by the *Gaia* Data Processing and Analysis Consortium (DPAC). Funding for the DPAC was provided by national institutions, in particular the institutions participating in the *Gaia* Multilateral Agreement. The *Gaia* mission website is https://www.cosmos.esa.int/gaia. The *Gaia* archive website is https://archives.esac.esa.int/gaia.

This research was funded in whole or in part by UK Research and Innovation (UKRI grants ST/X001121/1 and EP/X027562/1). The authors would like to thank the referee for their comments and suggestions that helped to improve the paper. For the purpose of open access, the author has applied a Creative Commons Attribution (CC BY) licence [where permitted by UKRI, 'Open Government Licence' or 'Creative Commons Attribution No-derivatives (CC BY-ND) licence' may be stated instead] to any Author Accepted Manuscript version arising from this submission.

DATA AVAILABILITY

All *TESS*-SPOC data are available from the NASA *MAST* portal, and *Gaia* DR2 and DR3 data are available from the *Gaia* archive. A copy of the full main-sequence *TESS*-SPOC FFI target sample (see Table 2) is available at CDS.

REFERENCES

Al-Wardat M. A., Hussein A. M., Al-Naimiy H. M., Barstow M. A., 2021, Publ. Astron. Soc. Aust., 38, e002
Babusiaux C. et al., 2018, A&A, 616, A10
Bailer-Jones C. et al., 2013, A&A, 559, A74
Battley M. P., Pollacco D., Armstrong D. J., 2020, MNRAS, 496, 1197
Belokurov V. et al., 2020, MNRAS, 496, 1922
Bryant E. M., Bayliss D., Van Eylen V., 2023, MNRAS, 521, 3663
Caldwell D. A. et al., 2020, Res. Notes Am. Astron. Soc., 4, 201
Davenport J. R., Mendoza G. T., Hawley S. L., 2020, AJ, 160, 36
Doyle L., Bagnulo S., Ramsay G., Doyle J. G., Hakala P., 2022, MNRAS, 512, 979
Eisner N. L. et al., 2021, MNRAS, 501, 4669
Gaia Collaboration, 2016, A&A, 595, A1
Gaia Collaboration, 2018, A&A, 616, A1
Gaia Collaboration, 2021, A&A, 649, A1
Gaia Collaboration, 2023, A&A, 674, A1
Gandolfi D. et al., 2018, A&A, 619, L10
Gilbert E. A. et al., 2020, AJ, 160, 116
Gill S. et al., 2020, ApJ, 898, L11

Gray D. F., 2021, The Observation and Analysis of Stellar Photospheres. Cambridge Univ. Press, Cambridge
Grellmann R., Preibisch T., Ratzka T., Kraus S., Helminiak K., Zinnecker H., 2013, A&A, 550, A82
Guerrero N. M. et al., 2021, ApJS, 254, 39
Huang C. X. et al., 2018, ApJ, 868, L39
IJspeert L. W., Tkachenko A., Johnston C., Garcia S., De Ridder J., Van Reeth T., Aerts C., 2021, A&A, 652, A120
Jenkins J. M., 2002, ApJ, 575, 493
Jenkins J. M. et al., 2010, in Radziwill N. M., Bridger A., eds, Proc. SPIE Conf. Ser. Vol. 7740, Software and Cyberinfrastructure for Astronomy. SPIE, Bellingham, p. 140
Jenkins J. M. et al., 2016, in Chiozzi G., Guzman J. C., eds, Proc. SPIE Conf. Ser. Vol. 9913, Software and Cyberinfrastructure for Astronomy IV. SPIE, Bellingham, p. 1232
Kunimoto M., Winn J., Ricker G. R., Vanderspek R. K., 2022, AJ, 163, 290
Leleu A. et al., 2021, A&A, 649, A26
Lendl M. et al., 2020, MNRAS, 492, 1761
Lindegren L. et al., 2018, Gaia technical note: GAIA-C3-TN-LU-LL-124-01
Mann A. W. et al., 2022, AJ, 163, 156
Moe M., Di Stefano R., 2017, ApJS, 230, 15
Newton E. R. et al., 2019, ApJ, 880, L17
Oddo D. et al., 2023, AJ, 165, 134
Prša A. et al., 2022, ApJS, 258, 16
Raghavan D. et al., 2010, ApJS, 190, 1
Ricker G. R. et al., 2015, J. Astron. Telesc. Instrum. Syst., 1, 014003
Sana H. et al., 2012, Science, 337, 444
Smith J. C., Morris R. L., Jenkins J. M., Bryson S. T., Caldwell D. A., Girouard F. R., 2016, PASP, 128, 124501
Söderhjelm S., 1999, A&A, 341, 121
Stassun K. G. et al., 2018, AJ, 156, 102
Stassun K. G. et al., 2019, AJ, 158, 138
Sullivan P. W. et al., 2015, ApJ, 809, 77
Taylor M. B., 2005, in Shopbell P., Britton M., Ebert R., eds, ASP Conf. Ser. Vol. 347, Astronomical Data Analysis Software and Systems XIV. Astron. Soc. Pac., San Francisco, p. 29
Tian Z.-J. et al., 2018, Res. Astron. Astrophys., 18, 052
Twicken J. D. et al., 2018, PASP, 130, 064502
Yee S. W. et al., 2022, AJ, 164, 70
Zinnecker H., 2003, in van der Hucht K., Herrero A., Esteban C., eds, Proc. IAU Symp. 212, A Massive Star Odyssey: From Main Sequence to Supernova. Astron. Soc. Pac., San Francisco, p. 80

This paper has been typeset from a TEX/LATEX file prepared by the author.